In Situ Spectroscopic Evidence for Neptunium(V)-Carbonate Inner-Sphere and Outer-Sphere Ternary Surface Complexes on Hematite Surfaces

YUJI ARAI,*,[†] P. B. MORAN,[‡,§]
B. D. HONEYMAN,[‡] AND J. A. DAVIS[†]

Department of Entomology, Soils and Plant Sciences, 270 Poole Agricultural Center, Clemson University, Clemson, South Carolina 29634-0315, Department of Environmental Science & Engineering, Colorado School of Mines, Coolbaugh Hall, Golden, Colorado 80401-1887, and Department of Chemistry and Geochemistry, Colorado School of Mines, Golden, 1500 Illinois Street, Golden, Colorado 80401

Np(V) surface speciation on hematite surfaces at pH 7−9 under pCO$_2$ = 10$^{-3.45}$ atm was investigated using X-ray absorption spectroscopy (XAS). In situ XAS analyses suggest that bis-carbonato inner-sphere and tris-carbonato outer-sphere ternary surface species coexist at the hematite−water interface at pH 7−8.8, and the fraction of outer-sphere species gradually increases from 27 to 54% with increasing pH from 7 to 8.8. The results suggest that the heretofore unknown Np(V)−carbonato ternary surface species may be important in predicting the fate and transport of Np(V) in the subsurface environment down gradient of high-level nuclear waste respositories.

Introduction

[237]Neptunium (Np) is present in low concentrations in high-level nuclear waste, but because of its long half-life, high radiotoxicity, and low sorption reactivity, it is considered an important radionuclide that may govern radiation exposure to humans several thousands of years after repository closure (*1*). Proposed underground storage of long-lived actinide isotope waste (*2*) raises questions about the long-term fate of transuranic elements in deep geologic repositories (e.g., Yucca Mountain, NV). Np(V) is expected be highly soluble and mobile in low-temperature aqueous-geochemical environments (*3*). Thus, knowledge of mineral−water interfacial speciation of Np is critical in assessing the long-term risk related to the fate and transport of this element. In oxic environments, Np is typically present in the pentavalent oxidation state (*2*, *4*), and adsorption of the neptunyl oxocation (Np(V)O$_2^{2+}$) on mineral surfaces presumably retards Np(V) transport in subsurface environments (*5*). Several researchers have investigated Np(V) adsorption on aluminum oxide, silica, kaolinite, montmorillonite, magnetite, hematite, hydrous aluminum oxide, hydrargillite, man-

ganite, and hausmanite (*6*−*16*) and natural sediments/soils (*10*, *17*−*20*). Effects of pCO$_2$ and pH on Np(V) adsorption on hematite/amorphous iron oxyhydroxide/manganite/hausmanite surfaces were previously studied. Whereas Np(V) sorption generally increased with increasing pH in a carbonate-free system, adsorption only occurs at pH 7−9.5 in air-equilibrated systems (*7*, *9*, *10*, *15*, *16*). Previous surface complexation model studies by Kohler et al.(*9*) indirectly suggested the presence of inner-sphere Np(V)−carbonate ternary species on hematite/goethite surfaces in air-equilibrated systems. However, no molecular-scale evidence has been reported to support the theory, while several XAS studies have frequently documented the formation of U(VI)−carbonato ternary surface species on hematite/imogolite/calcite surfaces (*21*−*24*). Carbonate is one of most important ligands that affects Np(V) speciation in groundwater because of its common abundance and its propensity to form aqueous carbonate complexes (*25*, *26*). In this study, we hypothesize the formation of Np(V)−carbonato ternary surface species on hematite surfaces. To test the hypothesis, surface speciation was examined as a function of pH using extended X-ray absorption fine structure spectroscopy.

Materials and Methods

Hematite was synthesized using the method described by Matijevic and Scheiner (*27*). Hematite precipitates were kept in low ionic strength solution (≤0.001 M NaClO$_4$) prior to use. The N$_2$ Brunauer−Emmett−Teller (BET) surface area of the freeze-dried powders was 43.8 m^2/g. Powder XRD showed that the hematite was crystalline with no evidence for goethite. The isoelectric point occurs at pH ∼ 9.8.

The neptunium-237 ([237]Np) stock solution, in secular equilibrium with its daughter protactinium-233 ([233]Pa), was prepared in 4 M nitric acid by Isotope Products Laboratories. With the exception of [233]Pa, the [237]Np solution was free of radioimpurities.

Samples were analyzed using a Beckman Coulter DU 800 UV/vis spectrophotometer with a wavelength interval of 0.1 nm and a scanning speed of 120 nm min^{-1}. Each sample cell was made of optical glass with a 10 mm path length and a septum sealable opening. Near-infrared (NIR) spectroscopic analysis showed that a dilute [237]Np stock solution (2 × 10^{-4} M in 20 mM nitric acid) consists of the pentavalent oxidation state. A characteristic band at 980 nm and a small band at 617 nm confirm the presence of the uncomplexed neptunyl (NpO$_2^+$) species. The spectrum lacked any evidence of the characteristic absorption bands for Np(IV) at 723 and 960 nm.

Speciation Calculations. Aqueous speciation calculations were completed with the equilibrium speciation program, FITEQL 4.0 (*28*), and the neptunium thermodynamic data given in Guillamont et al. (*29*). Supporting Information (SI-1) lists the relevant Np(V) thermodynamic data used in the calculations.

Extended X-ray Absorption Fine Structure Spectroscopic Measurements. Np(V) surface speciation on hematite surfaces was studied as a function of pH (7, 8, and 9) under the following reaction conditions: suspension density = 0.3 g L^{-1}, [Np]$_T$ = 4−5 μM, 22 (±2) °C, and I = 0.1 M NaClO$_4$. In addition to samples, Np(V) retention in controls and filteration equipment was tested. We found negligible amount of adsorption in these systems. Sufficient amounts of 10 mM NaHCO$_3$ solution were added to achieve the desired bicarbonate concentration in equilibrium with the partial pressure of carbon dioxide gas in air (pCO$_2$ = 10$^{-3.45}$ atm) at specified experimental pH values.

* Corresponding author phone: (864)656-2607; fax: (864)656-3443; e-mail: yarai@clemson.edu.

† Clemson University.

‡ Department of Environmental Science & Engineering, Colorado School of Mines.

§ Department of Chemistry and Geochemistry, Colorado School of Mines.

TABLE 1. Least-Squares Analyses of Np L$_{III}$-Edge Bulk XAS Spectra[a]

samples		O_{ax}	O_{eq}	C	Fe	O_{ax} MS	O_{dist}MS	F_{bin}	F_{mono}	F_{bis}	F_{tris}	R factor	log SI
pH 6.98	CN	2*	6(1)	----	1*	2*	----	0	0	0.73(±0.25)	0.27(±0. 25)	0.0158	−0.124
[Np(V)]$_i$ = 5	R (Å)	1.875(5)	2.47(1)	2.95(3)	3.45(2)	3.750	4.26(6)						−2.769
Γ = 2052	σ^2 (Å^2)	0.001(3)	0.009(2)	0.007*	0.005*	0.002	0.008*						−3.624
pH 8.28	CN	2*	5.1(9)	----	1*	2*	----	0	0	0.61(±0.25)	0.39(±0.25)	0.0034	0.708
[Np(V)]$_i$ = 4	R (Å)	1.886(5)	2.49(1)	2.90(3)	3.47(3)	3.772	4.21(5)						−0.63
Γ = 1636	σ^2 (Å^2)	0.0012(3)	0.0081(2)	0.007*	0.005*	0.0023	0.008*						−2.792
pH 8.81	CN	2*	5(1)	----	1*	2*	----	0	0	0.46(±0.23)	0.54(±0.23)	0.0134	0.454
[Np(V)]$_i$ = 5	R (Å)	1.887(6)	2.49(1)	2.93(3)	3.41(3)	3.775	4.23(5)						−0.32
Γ = 944	σ^2 (Å^2)	0.0012(4)	0.009(2)	0.007*	0.005*	0.0025	0.008*						−3.046

[a] CN: Coordination number. R: Interatomic distance (Å). σ^2: Debye−Waller factor (Å^2). [Np(V)]$_i$: Initial Np(V) concentrations (μM). Γ: Surface coverage (mg kg^{-1}). Fit quality confidence limit for parameters: Np−C/Fe shell CN: ±10% (Clark et al., 1996), *: Fixed parameter. Parameters for three O_{dis} MS paths are summarized into one. F_{bin}, F_{mono}, F_{bis}, and F_{tris}: Fraction of binary, mono-, bis-, and tris-carbonate Np(V) ternary surface species. Saturation index values (Log SI) were estimated for crystalline NpO$_2$(s), (Log K = −1.8 (37)), crystalline NaNpO$_2$CO$_3$·3.5H$_2$O(s) (Log K = −11.156 (29)) and am. NpO$_2$OH(S) (Log K = −5.3 (37)) (from top to bottom; NpO$_2$(S), crystalline NaNpO$_2$CO$_3$·3.5H$_2$O(S), and am. NpO$_2$OH(S)).

With use of aqueous speciation calculations, these systems were calculated to be undersaturated with respect to amorphous NpO$_2$OH (s) and crystalline NaNpO$_2$CO$_3$·3.5H$_2$O (s) at all three pH values (Table 1), and neptunyl hydroxide NpO$_2$(s) at pH 6.98, but slightly supersaturated for neptunyl oxide, NpO$_2$(s), at pH 8.28 and 8.81 (Table 1). However, Np(V) hydroxide precipitates were not observed in any of the samples, as indicated by the results of our XAS analyses (see the Results and Discussion section), and this result is likely by kinetic limitations in the precipitation of crystalline Np(V) oxides.

Samples were prepared in 1 L polycarbonate bottles. Samples were stirred under humidified air for 24 h prior to Np(V) addition. During this pre-equilibration, each sample pH was periodically adjusted to the desired value. After 24 h, a 0.036 M acidic Np(V) stock solution was slowly added to each sample (30 μL or less at time) to avoid local saturation. The samples were stirred for an additional 24 h while being maintained at the chosen pH values. Small aliquots were passed through 0.1 μm Acrodisc syringe filters and analyzed for alpha activity by a Packard 2500TR liquid scintillation counting (LSC) system and Ultima Gold XR LSC cocktail. Sorption was determined by difference using the total and final Np(V) solution activities with a relative standard deviation of ±1%. A Thermo Orion Ross combination electrode calibrated with NIST certified pH buffers (4.000, 7.000, and 10.000) was used for all pH measurements. Sample pH was adjusted using hydrochloric acid and sodium hydroxide. The bulk of the solution phase was decanted and the remaining sample suspensions were centrifuged at 10000 rpm for 60 min.

The samples were loaded in custom-designed sample cells that consist of 3 mm Delrine sample holders, which were then sealed with Mylar/polycarbonate windows and two additional aluminum containments. Room-temperature Np L$_{III}$ edge (17610 eV) fluorescence spectra were collected at the Stanford Synchrotron Radiation Laboratory (SSRL) beamline 11.2 (Si(220) double crystal monochromator) using a Canberra 13-element Ge detector array equipped with a Y 6μx filter and several Al foils. A zirconium reference foil was used to calibrate at the Zr K-edge absorption edge energy positions (17998 eV).

The program FEFF 6 (30) was used to estimate backscattering phases and amplitude functions of single scattering (SS) Np−O$_{ax}$, Np−O$_{eq}$, Np−C, and transdioxo Np−O$_{ax}$ multiple scattering paths (MS), which were derived from structural refinement data for Np substituted andersonite (Na$_2$CaNpO$_2$(CO$_3$)$_3$·5.33H$_2$O) (31). A Np−Fe SS path was estimated from the structural refinement data of Np/Fe substituted phuralumite (Fe$_2$(OH)$_2$(PO$_4$)$_2$(NpO$_2$)$_3$(OH)$_4$·10H$_2$O) (32). XAS data reduction and analyses were performed using the IFEFFIT engine based interface, SixPACK (33). k^3-weighted Fourier-transformed XAS spectra were fit in R-space over the range of 1−4.5 Å.

In the fit, fixed values for CN and R values for transdioxo neptunium MS paths (Np=O$_{ax1}$=Np=O$_{ax2}$) was correlated with SS of Np=O$_{ax}$, and σ^2 of transdioxo MS paths were estimated using the similar theoretical calculation described in Hudson et al. (34) (2 × σ^2_{oax} and 2 × R_{oax}). ΔE_o was allowed to float and linked to all shells during the fit. To compare the differences in fit, unfixed σ^2 values for Np−C and Np−Fe shells from the preliminary fit were averaged, and these values (i.e., Np−C: 0.007 and Np−Fe: 0.005) were used for all samples. To account for the changes in amplitude of two Np−O$_{dist}$ MS paths (3 and 4 legged), SS and MS contributions of distal oxygen (O$_{dist}$) atom of carbonate ions ((1) Np−O$_{dist}$ ss, (2) Np−C−O$_{dist}$ (3 legged MS), and (3) Np−C−O$_{dist}$ (4 legged MS)) were included in the fit with a Np−O$_{dist}$ SS path. The σ^2 for Np−O$_{dist}$ MS paths were explicitly calculated from σ^2 of Np−O$_{dist}$ SS path by summing the disorder parameters of each SS path (Hudson et al., 1996). Based on the following assumptions, $\sigma^2_{c-o} \ll \sigma^2_{odist} = \sigma^2_{Np-c}$ (0.007 Å^2), σ^2 for Np−O$_{dist}$ MS paths was fixed at 0.008 Å^2.

A maximum of four putative surface species (binary, mono-carbonato, and bis-carbonato inner-sphere, and tris-carbonato outer-sphere surface species) were considered in the fit as Arai and co-workers have previously demonstrated in the XAS analyses of U(VI) adsorbed on imogolite surfaces (21). Amplitude reduction factors for Np−C and O$_{dist}$ shells were assumed to originate from four different fractions (F) of Np surface species (i.e., binary (F$_{bin}$), mono-carbonato (F$_{mono}$), and bis-carbonato inner-sphere (F$_{bis}$), and tris-carbonato outer-sphere surface species (F$_{tris}$)). Based on the assumption, we set the "total fraction (F) = 1" as a summation of all fractions of surface species (i.e., 1 = F_{bin} + F_{mono} + F_{bis} + F_{tris}). The fractions for each mono- and bis-carbonato species (i.e., Np−C SS and Np−O$_{dist}$ SS) were defined as "F_{mono}*S$_o^2$*1" and "S$_o^2$*F_{bis}*2", respectively. For the tris-carbonato outer-sphere surface species, "S$_o^2$*F_{tris}*3" was used only for defining the Np−C SS and Np−O$_{dist}$ SS paths. Based on a preliminary fit, we found a Np−Fe interatomic distance (∼3.45 Å) corresponding to inner-sphere Np bidentate mononuclear coordination with the iron octahedral structure (i.e., one Fe atom is coordinated). Therefore, we used "S$_o^2$*1*F_{bin}", "S$_o^2$*1*F_{mono}" and "S$_o^2$*1*F_{bis}" for the Np−Fe path for non-, mono-, and bis-carbonato inner-sphere surface species, respectively.

To facilitate the comparison under different reaction conditions, coordination numbers and Debye−Waller factors for some shells were fixed (i.e., CN of Np−O$_{ax}$: 2, σ^2 of Np−C; 0.007 Å^2, σ^2 of Np−Fe; 0.005). S_o^2 was fixed at 0.9. The other coordination numbers, Debye−Waller factors, and interatomic distances were allowed to vary.

Results and Discussion

Neptunyl Aqueous Speciation Calculations. Equilibrium speciation calculations were conducted for the reaction
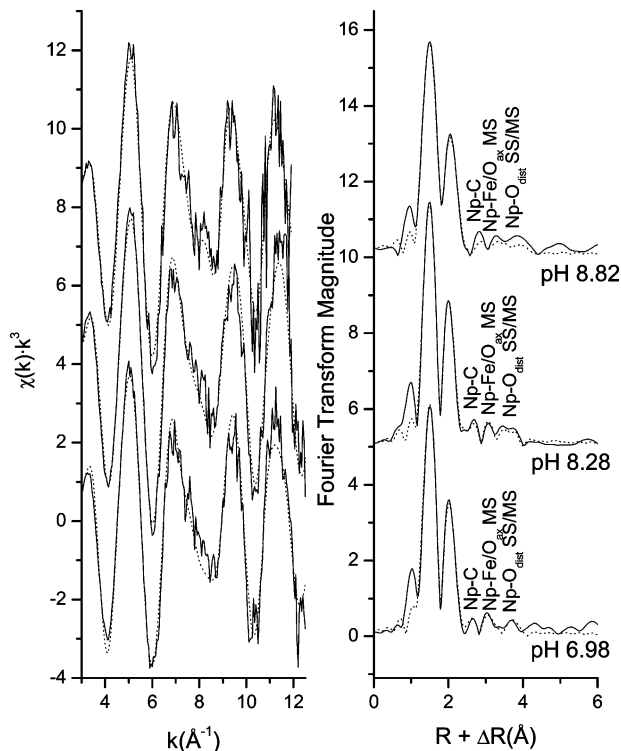
FIGURE 1. (a) Normalized, background-subtracted k^3-weighted Np L_{III}-edge EXAFS spectra of Np(V)-adsorbed hematite samples in air; (b) Fourier-transformed k^3-weighted Np L_{III}-edge EXAFS spectra of Np(V)-adsorbed hematite (solid lines) and nonlinear least-squares fits (dotted lines).
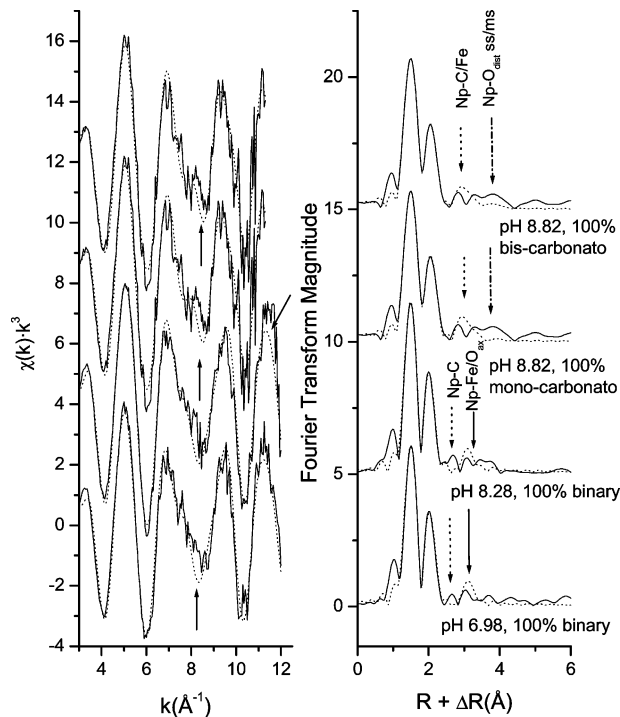

FIGURE 2. (a) Normalized, background-subtracted k^3-weighted Np L_{III}-edge EXAFS spectra of Np(V)-adsorbed hematite samples in air; (b) Fourier-transformed k^3-weighted Np L_{III}-edge EXAFS spectra of Np(V)-adsorbed hematite. Solid lines are the experimental data and the dotted lines represent fits with fixed fractions of binary, mono-carbonato, and bis-carbonato inner-sphere surface species. Dotted, dash, solid, and dash-dot arrows indicate Np−C, Np−C/Fe, Np−Fe/O$_{trans}$ MS, and Np−O$_{dist}$ SS/MS shells.

conditions ([Np(V)] = 4 μM, I = 0.1 M NaClO$_4$, 25 °C, and pCO$_2$ = $10^{-3.5}$atm) in XAS sample preparation. The results show that the predominant Np(V) aqueous species is NpO$_2^{2+}$ at pH 4−8, and the activity of carbonato complexes (i.e., NpO$_2$(CO$_3$)$_2$OH^{4-}, NpO$_2$(CO$_3$)$_2^{3-}$, and NpO$_2$CO$_3^-$, and NpO$_2$-(CO$_3$)$_3^{5-}$) gradually become significant aqueous species at pH > 7.5 (SI-2).

Extended X-ray Absorption Fine Structure Analyses. Figures 1a and 1b show the k^3-weighted EXAFS spectra of Np(V)-adsorbed hematite samples. Fit results are shown in Table 1 (in units of Å). Interatomic distances are corrected for phase shift unless otherwise mentioned in the text. The structural parameters of all samples contain two axial oxygen distances at approximately 1.88 Å and five to six equatorial oxygen distances at ~2.5 Å, indicating the presence of a O=Np(V)=O transdioxo structure. No loss of axial oxygen atoms indicate that beam-induced reduction of Np(V) did not occur during the XAS data collection. These Np−O$_{ax}$/O$_{eq}$ distances can be clearly observed in the Fourier transforms (FTs) at ~1.75 and 2 Å, $R + \Delta R$ (Figure 1b). Additional FT peaks are also observed at ~2.6, 3.1, and 3.8 Å, $R + \Delta R$, which can be attributed to C, Fe, and distal O (in carbonate groups) shells, as described below.

As reported in a previous XAS study of Np(V)−carbonate (aq) complexes at pCO$_2$ = $10^{-3.45}$ atm (25), the distance at ~2.6 Å, $R + \Delta R$, corresponds to a carbonate ligand coordination of the Np(V) atom in a bidentate fashion having a Np−C distance of ~2.9 Å. Estimated distances are in good agreement with the results of Np(V)−carbonate aqueous species (i.e., NpO$_2$(CO$_3$)$^-$, NpO$_2$(CO$_3$)$_2^{3-}$, and NpO$_2$(CO$_3$)$_3^{5-}$) (25). The presence of inner-sphere surface species can also be suggested in the residual Fourier transform Np−Fe peaks (SI-3) which were prepared by subtracting the SS contributions of Np−O$_{ax}$, Np−O$_{eq}$, Np−C, and Np− O$_{dist}$, and the MS contributions of one Np=O$_{ax}$ and two Np−O$_{dist}$ from

normalized spectra. All three samples contain the Np−Fe peaks (SI-3).

The FT frequency at ~3.1 Å, $R + \Delta R$, is fit well with Fe neighbors at ~3.45 Å, suggesting the formation of inner-sphere bidentate mononuclear surface species on iron octahedral structures. The FT frequency at ~3.8 Å, $R + \Delta R$, is attributed to SS and MS paths of the Np−O$_{dist}$ at ~4.2 Å. Clark and co-workers have shown the importance of the Np−O$_{dist}$ scattering paths in Np(V)−carbonate aqueous species (25). Our observation of the Np−O$_{dist}$ contribution from the Np(V)−carbonato ternary species at the mineral−water interface adds new insight to the types of Np(V) surfaces that may form in low-temperature geochemical environments.

Prior to incorporating the various combinations of binary and carbonate ternary surface species in the fit, we attempted a fit with the analogous predominant aqueous species at each pH value. For example, based on the Np(V)(aq) speciation diagram (SI-2), we assumed that 100% of the surface species were binary at pH ~ 7−8 and 100% of mono-carbonato or bis-carbonato surface species (Figures 2a and 2b) at pH ~ 9. The results of these fit attempts are presented in Figures 2a and 2b. k^3-weighted EXAFS spectra clearly indicate a poor fit at $k \sim 8$ Å^{-1} in pH 6.98 and 8.82 spectra (indicated by arrows in Figure 2a) and at $k \sim 11$ Å^{-1} in the pH 8.2 spectrum (arrow in Figure 2a). The poor fits are clearly observed in all FT spectra (Figure 2b). Np−Fe shells are overestimated (as indicated by solid-line arrows in Figure 2b), suggesting that the fraction of inner-sphere surface species are overestimated. This indicates that some fraction of outer-sphere surface species (e.g., tris-carbonato outer-sphere surface species) might need to be considered in the fit.

In pH 6.98−8.81 samples, underestimated Np−C shells suggest that Np coordination by carbonate ligand in the
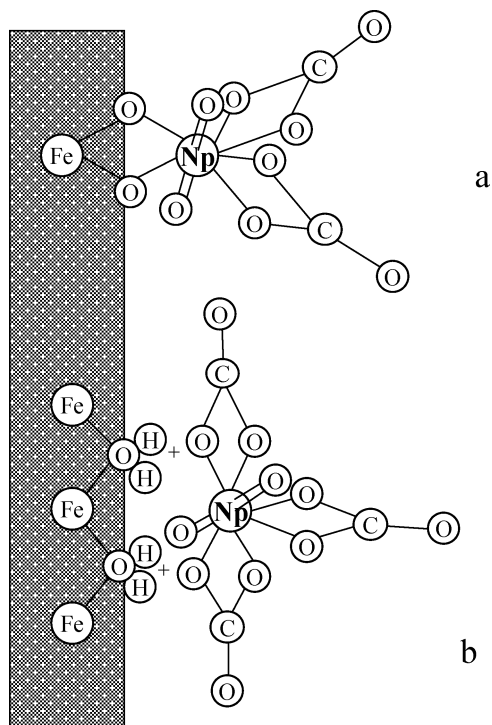
FIGURE 3. Ball-and-stick representation of Np(V) surface species on the iron octahedral structure of hematite based on the results of XAS analyses shown in Table 1. (a) Bis-carbonato$-$Np(V) inner-sphere ternary complex via bidentate mononuclear Np(V)$-$O$_2$$-$Fe linkage. (b) Tris-carbonato$-$Np(V) outer-sphere ternary complex.

surface species might be greater than observed in aqueous solution at the same pH value. Furthermore, the fit quality for distal oxygen shells becomes poor as pH increases from 7 to 8.8 (indicated by dash-dot arrows in Figure 2b). Previous XAS studies suggested inner-sphere binary surface species occurred on goethite surface at pH $\sim$ 7 (35); however, our preliminary XAS analyses indicates that neptunyl$-$carbonato ternary species occur on hematite surfaces. The chemical environment at the mineral$-$water interface is apparently sufficiently different (e.g., electrical double layer, solvation energy, and dielectric constant of solvent at interface) to favor these species at pH values lower than those observed in water. Consequently, Np$-$C/Fe/O$_{dist}$ coordination number correlated analyses were conducted to simultaneously consider the four putative species mentioned earlier.

To compensate for the overpredicted Np$-$Fe shell (i.e., inner-sphere surface species) and underpredicted U$-$C shell at pH $\sim$ 7 (the bottom spectrum in Figure 3b), we considered tris-carbonato surface species along with three inner-sphere species (binary, mono-carbonato, and bis-carbonato) in the fit. A combination of bis-carbonato inner-sphere and tris-carbonato outer-sphere surface species yielded the best fit (R factor: 0.0158) (Figures 1a and 1b), resulting in 73% of bis-carbonato inner-sphere and 27% of tris-carbonato outer-sphere surface species (Table 1).When binary or mono-carbonato inner-sphere surface species were included with the tris-carbonato surface species, the amplitude of Np$-$C shell was slightly underpredicted.

Similarly, the best fit (R factor = 0.0034) was obtained for the pH 8.28 sample when a combination of bis-carbonato inner-sphere and tris-carbonato outer-sphere surface species were considered (Figures 1a and 1b). The fraction of inner-sphere bis-carbonato surface species slightly reduced to 61% and the fraction of outer-sphere surface species increased to 39%. An increase in the fraction tris-carbonato surface species (i.e., an increase in carbonate ligand coordination)

can be seen in the enhanced FT feature at $\sim$3.8 Å, $R + \Delta R$ (Figure 1b).

In the pH 8.82 sample, the strong distal oxygen SS/MS contribution at $\sim$3.8 Å, $R + \Delta R$, is clearly seen (Figure 1b). 54% of the surface Np(V) was adsorbed as the tris-carbonato outer-sphere surface species, with approximately 46% of adsorbed Np(V) present as bis-carbonato inner-sphere ternary species (Table 1). As was demonstrated for U(VI) sorption on imogolite (21), an outer-sphere tris-carbonato species forms at alkaline pH values where a combination of factors contribute to its relative stability: (1) the activity of carbonate is increasing in solution, (2) the stability of inner-sphere species is decreasing due to increasing pH, and (3) the surface charge is still positive because the pH is below the PZC.

As Arai and co-workers have previously demonstrated, the use of coordination number-correlated XAS analyses on U(VI)-reacted imogolite (21), a similar model was successfully applied here to elucidate Np(V) surface species at the hematite$-$water interface. We found that Np(V)$-$carbonato species, which have previously only been documented as aqueous species (25), readily form on hematite surfaces as ternary species at pH 7$-$9 in air-equilibrated systems. The stabilities of both surface species (relative to aqueous species) are likely to be very dependent on aqueous chemical conditions, especially the concentration of bicarbonate in groundwater and other solutes that influence surface charge at the mineral$-$water interface. The variable chemistry of the groundwater environments down gradient of the Yucca Mountain high-level waste disposal site and its potential impact on K_d values for Np(V) sorption have been discussed by Turner et al. (1). The results presented here demonstrate that the stability of surface species for Np(V) sorption will be sensitive to aqueous chemical conditions in the groundwater because the carbonate anion is a component of the predominant surface and aqueous complexes. As in the case of U(VI) (36), this means that reactive transport model simulations that describe the fate of transport of Np(V) in the environment down gradient of the Yucca Mountain site would have a stronger technical basis if the conceptual model for sorption was represented by surface complexation (coupled with aqueous chemistry) rather than a constant K_d-modeling approach.

Note Added after ASP Publication

This paper was published ASAP May 4, 2007 with a minor error in the y-axis labels of Figures 1 and 2; the corrected version was published ASAP May 9, 2007.

Supporting Information Available

In SI-1, -2, and -3, formation constants for aqueous species, Np(V) aqueous speciation diagram, and Fourier-transformed

XAS spectra of residual Np−Fe shells, respectively, are provided. This material is available free of charge via the Internet at http://pubs.acs.org.

Literature Cited

(1) Turner, D. R.; Bertetti, F. P.; Pabalan, R. T. Role of radionuclide sorption in high-level waste performance assessment: Approaches for the abstraction of detailed models. In *Geochemistry of Soil Radionuclides*; Zhang, P.-C., Brady, P. V., Eds.; Soil Science Society of America: Madison, WI, 2002; pp 211−252.

(2) Dozol, M.; Hagemann, R.; Radionuclide migration in groundwaters: Review of the behavior of actinides. *Pure Appl. Chem.* **1993**, *65*, 1081−1102.

(3) Nitsche, H.; Lee, S. C.; Gatti, R. C. Determination of plutonium oxidation states at tracer levels pertinent to nuclear waste disposal. *J. Radioanal. Nucl. Chem.-Art.* **1988**, *124*, 171−185.

(4) Runde, W. The chemical interactions of actinides in the environment. *Los Alamos Sci.* **2000**, *26*, 392−411.

(5) Viswanathan, H. S.; Robinson, B. A.; Valocchi, A. J.; Triay, I. R. A reactive transport model of neptunium migration from the potential repository at Yucca Mountain. *J. Hydrol.* **1998**, *209* (1), 251−280.

(6) Aksoyoglu, S.; Burkart, W.; Goerlich, W. Sorption of Neptunium on Clays. *J. Radioanal. Nucl. Chem.-Art.* **1991**, *149* (1), 119−122.

(7) Girvin, D. C.; Ames, L. L.; Schwab, A. P.; McGarrah, J. E. Neptunium adsorption on synthetic amophous iron oxyhydroxide. *J. Colloid Interface Sci.* **1991**, *141* (1), 67−78.

(8) Bradbury, M. H.; Baeyens, B. Modelling the sorption of Mn(II), Co(II), Ni(II), Zn(II), Cd(II), Eu(III), Am(III), Sn(IV), Th(IV), Np(V) and U(VI) on montmorillonite: Linear free energy relationships and estimates of surface binding constants for some selected heavy metals and actinides. **2005**, *69*, 875−892.

(9) Kohler, M.; Honeyman, B. D.; Leckie, J. O. Neptunium(V) sorption on hematite (α-Fe_2O_3) in aqueous suspension: The effect of CO_2. *Radiochim. Acta* **1999**, *85* (33−48).

(10) Li, W. J.; Tao, Z. Y.; Guo, G. L.; Li, S. S. Sorption and desorption of neptunium(V) on loess: batch and column experiments *Radiochim. Acta* **2003**, *91* (10), 575−582.

(11) Nakata, K.; Fukuda, T.; Nagasaki, S.; Tanaka, S.; Suzuki, A.; Tanaka, T.; Muraoka, S. Sorption of neptunium on iron-containing minerals. *Czech. J. Phys.* **1999**, *49* (1), 159−166.

(12) Nakata, K.; Nagasaki, S.; Tanaka, S.; Sakamoto, Y.; Tanaka, T.; Ogawa, H. Sorption and desorption kinetics of Np(V) on magnetite and hematite. *Radiochim. Acta* **2000**, *88* (8), 453−457.

(13) Nakata, K.; Nagasaki, S.; Tanaka, S.; Sakamoto, Y.; Tanaka, T.; Ogawa, H. Sorption and reduction of neptunium(V) on the surface of iron oxides *Radiochim. Acta* **2002**, *90* (9−11), 665−669.

(14) Tochiyama, O.; Endo, S.; Inoue, Y. Sorption of neptunium(V) on various iron-oxides and hydrous iron-oxides. *Radiochim. Acta* **1995**, *68* (2), 105−111.

(15) Turner, D. R.; R. T. P.; Bertetti, F. P. Neptunium(V) sorption on montmorillonite; an experimental and surface complexation modeling study. *Clays Clay Miner.* **1998**, *46* (3), 256−269.

(16) Wilk, P. A.; Shaughnessy, D. A.; Wilson, R. E.; Nitsche, H. Interfacial Interactions between Np(V) and Manganese Oxide Minerals Manganite and Hausmannite. *Environ. Sci. Technol.* **2005**, *39* (8), 2608−2615.

(17) Mincher, B. J.; Fox, R. V.; Cooper, D. C.; Groenewold, G. S. Neptunium and plutonium sorption to Snake River Plain, Idaho soil *Radiochim. Acta* **2003**, *91* (7), 397−401.

(18) Braithwaite, A.; Richardson, S.; Moyes, L. N.; Livens, F. R.; Bunker, D. J.; Hughes, C. R.; Smith, J. T.; Hilton, J. Sorption kinetics of uranium-238 and neptunium-237 on a glacial sediment. *Czech. J. Phys.* **2000**, *50* (2), 265−269.

(19) DelNero, M.; Made, B.; Bontems, G.; Clement, A. Adsorption of neptunium(V) on hydrargilite. *Radiochim. Acta* **1997**, *76* (4), 219−228.

(20) Hart, K. P.; Payne, T. E.; Robinson, B. J.; Vaniseghem, P. Neptunium uptake on Boom Clay-time dependence and association of Np with fine particles. *Radiochim. Acta* **1994**, *66* (7), 19−22.

(21) Arai, Y.; McBeath, M.; Bargar, J. R.; Joye, J.; Davis, J. A. Uranyl adsorption and surface speciation at the imogolite-water interface: Self-consistent spectroscopic and surface complexation models. *Geochim. Cosmochim. Acta* **2006**, *70* (10), 2492−2509.

(22) Bargar, J. R.; Reitmeyer, R.; Davis, J. Spectroscopic confirmation of uranium(VI)-carbonate adsorption complexes on hematite. *Environ. Sci. Technol.* **1999**, *33* (14), 2481−2484.

(23) Bargar, J. R.; Reitmeyer, R.; Lenhart, J. J.; Davis, J. A. Characterization of U(VI)-carbonato ternary complexes on hematite: EXAFS and electrophoretic mobility measurements. *Geochim. Cosmochim. Acta* **2000**, *64* (16), 2737−2749.

(24) Elzinga, E. J.; Tait, C. D.; Reeder, R. J.; Rector, K. D.; Donohoe, R. T.; Morris, D. E. Spectroscopic investigation of U(VI) sorption at the calcite-water interface. *Geochim. Cosmochim. Acta* **2004**, *68* (11), 2437−2448.

(25) Clark, D. L.; Conradson, S. D.; Ekberg, S. A.; Hess, N. J.; Neu, M. P.; Palmer, P. D.; Runde, W.; Tait, C. D. EXAFS studies of pentavalent neptunium carbonate complexes. Structural elucidation of the principal constituents of neptunium in groundwater environments. *J. Am. Chem. Soc.* **1996**, *118*, 2086−2090.

(26) Clark, D. L.; Hobart, D. E.; Neu, M. P. Actinide carbonate complexes and their importance in actinide environmental chemistry. *Chem. Rev.* **1995**, *95*, 25−48.

(27) Matijevic, E.; Scheiner, P. Ferrous hydrous oxide sols III. Preparation of uniform particles by hydrolysis of Fe(III)-chloride, -nitrate, and −perchlorate solutions. *J. Colloid Interface Sci.* **1978**, *63*, 509−524.

(28) Herbelin, A. L.; Westall, J. C. *FITEQL: A computer program for the determination of chemical equilibrium constants from experimental data, Version 4.0*, 99-01; Oregon State University: Corvallis, OR, 1999.

(29) Guillaumont, R.; Fanghanel, T.; Neck, V.; Fuger, J.; Palmer, D. A.; Grenthe, I.; Rand, M. H. *Chemical Thermodynamics 5: Update on the chemical thermodynamics of uranium, neptunium, plutonium, americium, and technetium*; Elsevier: Amsterdam, 2003.

(30) Rehr, J. J.; Albers, R. C.; Zabinsky, S. I. High-order multiple scattering calculations of x-ray absorption fine structure. *Phys. Rev. Lett.* **1992**, *69*, 3379−3400.

(31) Mereiter, K. Neue kristallographische daten ueber das uran-mineral andersonit. New crystalographic data of the uranium mineral andersonite. *Anz. Oesterr. Akad. Wiss., Math.-Naturwiss. Kl.* **1986**, *123* (3), 39−41.

(32) Piret, P.; Declercq, J.-P.; Wauters-Stoop, D. Structure of phuralumite. *Acta. Crystallogr., Sect. B: Struct. Sci.* **1979**, *35*, 1880−1882.

(33) Webb, S. M. A graphical user interface for XAS analysis using IFEFFIT. *Phys. Scr.* **2005**, (T115), 1011−1014.

(34) Hudson, E. A.; Allen, P. G.; Terminello, L. J.; Denecke, M. A.; Reich, T. Polarized x-ray absorption spectroscopy of the uranyl ion: Comparison of experiment and theory. *Phys. Rev. B* **1996**, *54*, 156−165.

(35) Combes, J.; Chisholm-Brause, C. J.; Brown, G. E. J.; PArks, G. A.; Conradson, S. D.; Eller, P. G.; Trlay, I. R.; Hobart, D. E.; Meijer, A. EXAFS spectroscopic study of neptunium(V) sorption at the α-FeOOH/water interface. *Environ. Sci. Technol.* **1992**, *26*, 376−382.

(36) Curtis, G. P.; Davis, J. A.; Naftz, D. L. Simulation of reactive transport of uranium(VI) in groundwater with variable chemical conditions. *Water Resour. Res.* **2006**, *42*, W04404 ; doi:10.1029/2005WR003979.

(37) Lemire, R. J.; Fuger, J.; Nitsche, H.; Potter, P.; Rand, M. H.; Rydberg, J.; Spahiu, K.; Sullivan, J. C.; Ullman, W. J.; Vitorge, P.; Wanner, H. *Chemical Thermodynamics 4. Chemical Thermodynamics of Neptunium and Plutonium*; Elsevier: Amsterdam, 2001.